ACADEMIC PRESS

Available online at www.sciencedirect.com
SCIENCE DIRECT®

NeuroImage

NeuroImage 20 (2003) 765–783

www.elsevier.com/locate/ynimg

Single-trial variability in early visual neuromagnetic responses: an explorative study based on the regional activation contributing to the N70m peak

N.A. Laskaris, L.C. Liu, and A.A. Ioannides*

Laboratory for Human Brain Dynamics, RIKEN Brain Science Institute (BSI), Wako-shi, Saitama 351-0198, Japan

Received 12 September 2002; revised 25 May 2003; accepted 11 June 2003

Abstract

Cortical activity evoked by repeated identical sensory stimulation is extremely variable. The source of this variability is often assigned to "random ongoing background activity" which is considered to be irrelevant to the processing of the stimuli and can therefore be eliminated by ensemble averaging. In this work, we studied the single-trial variability in neuromagnetic responses elicited by circular checkerboard pattern stimuli with radii of 1.8°, 3.7°, and 4.5°. For most of the MEG sensors over the occipital areas, the averaged signal showed a clear early (N70m) response following the stimulus onset and this response was modulated by the checkerboard size. A data-driven spatial filter was used to extract one of the many possible composite time courses of single-trial activity corresponding to the complex of N70m generators. Pattern analysis principles were then employed to analyze, classify, and handle the extracted temporal patterns. We explored whether these patterns correspond to distinct response modes, which could characterize the evoked response better than the averaged signal and over an extended range of latencies around N70m. A novel scheme for detecting and organizing the structure in single-trial recordings was utilized. This served as a basis for comparisons between runs with different checkerboard sizes and provided a causal interpretation of variability in terms of regional dynamics, including the relatively weak activation in primary visual cortex. At the level of single trial activity, the polymorphic response to a simple stimulus is generated by a coupling of polymodal areas and cooperative activity in striate and extrastriate areas. Our results suggest a state-dependent response with a wide range of characteristic time scales and indicate the ongoing activity as a marker of the responsiveness state.

Keywords: Magnetoencephalography (MEG); N70m; Single-trial analysis; Vector quantization; Visual evoked field; Human; Primary visual cortex (V1); Polymodal areas

Introduction

The single trial variability of sensory evoked responses in cortex has been the subject of many studies based on different sensory modalities and various neurophysiological or neuroimaging techniques including intracellular recordings (Azouz and Gray, 1999), single-unit recordings (Reich et al., 1997), recording of local field potentials (Kisley and Gerstein, 1999; Truccolo et al., 2002), optical imaging (Arieli et al., 1996), BOLD-fMRI (Duann et al., 2002), electroencephalography (EEG) (Mast and Victor., 1991; Brand, 1997; Jung et al., 2001; Lutz et al., 2002), and magnetoencephalography (MEG) (Liu and Ioannides, 1996; Liu et al., 1998; Ioannides et al., 1998). The major issue in all these studies is the validity of the "signal plus noise" model, i.e., whether a relative stereotyped evoked response is linearly superimposed on the ongoing brain activity after every stimulus presentation, a prerequisite for the validity of ensemble averaging. Experimental evidence supporting averaging as a response recovery technique can be claimed by many studies with EEG and MEG showing reproducible average responses in somatosensory, auditory, and visual cortices after averaging a large number of trials in single or

* Corresponding author. Laboratory for Human Brain Dynamics, RIKEN Brain Science Institute (BSI), 2-1 Hirosawa, Wako-shi, Saitama 351-0198, Japan. Fax: +81-48-467-9731.

E-mail address: ioannides@postman.riken.go.jp (A.A. Ioannides).

1053-8119/$ – see front matter © 2003 Elsevier Inc. All rights reserved.
doi:10.1016/S1053-8119(03)00367-7

multiple recordings. These studies have shown that there is a time-locked response that can be recovered by averaging. However, the comparison of the averaged signal with individual single trial responses suggests that the average is not a reflection of a unitary sequence of events but a mixture of different histories generated via a nonlinear coupling of stimulus evoked and ongoing activity. The motivations for the present study were the exploitation of the rich temporal information of MEG recordings for a detailed characterization of single-trial variability based on signal properties and the elucidation of the dominant sources contributing to this variability. We used simple visual stimuli and subjects whom we have previously studied with MEG and fMRI in order to define their early responses in the primary visual cortex (V1). This enabled us to scrutinize the relationship of the activity in the first cortical area excited by the stimulus with the response variability seen in the multichannel MEG signal.

The neural generators of early visual responses to pattern-onset stimulation in humans are still under debate and two recent excellent works can be used to illustrate the diversity of opinions that now prevail. In the first study by Russo et al. (2001), dipole modeling of the grand average (average across subjects) EEG signals was used to identify the sources with and without constraints from fMRI. This procedure led to the localization of the C1 source (~55 ms) within the calcarine fissure for both upper and lower field stimuli, without the need for position constraints. For stimuli in all quadrants, the next positive deflections of the grand average EEG signal were early (80–110 ms) and late (110–140 ms) P1 phases that localized to the lateral extrastriate cortex (BA18) and the ventral occipitotemporal cortex, respectively. In the second study by Foxe and Simpson (2002), the average high-density EEG signal was first transformed into a scalp current source map on the standard 10–20 system by Laplace transformation (Hjorth, 1975). The results of this study were not in agreement with the notion that the initial ERP component C1 (peaking between ~60 and 90 ms), represents V1 activation and that the ensuing P1 component (peaking between ~100 and 140 ms) represents subsequent extrastriate activation, suggesting instead a significantly condensed scenario for activation in the visual system, with even frontal areas showing activation by 85 ms. This fast scenario is consistent with data obtained from monkey intracranial recordings (Raiguel et al., 1989) and human ERP studies (Thorpe et al., 1996).

Three recent MEG studies have also addressed the question of early visual processing using the averaged MEG signal elicited by stimuli confined to quadrants or parts of quadrants of the visual field. In a pattern reversal stimulation paradigm (Vanni et al., 2001), the source of early MEG response (55–70 ms after stimulus onset) was localized first in primary visual areas, 3–4 ms later in the anteromedial part of the cuneus, and finally in many other areas. In another MEG study (Tzelepi et al., 2001), generators in both striate and extrastriate cortex were found to contribute to the formation of the early (N70m) peak following stimulation by sinusoidal grating pattern onset. Highly reproducible focal activity in V1/V2 was accompanied by a concurrent strong but labile activity in V5 and the human homologue of V6. In an attempt to precisely define the very early activity evoked by a visual stimulus, the MEG and fMRI localizations were compared for pattern onset stimuli confined to part of the lower field quadrant, selected so that the estimated V1 activation was well separated from the V2 representation of the same stimulus (Moradi et al., 2003). The study showed excellent agreement between tomographic estimates of activity (3–5 mm), for the very first entry to the visual system, typically 40 ms after the stimulus onset.

In the current study, we used two subjects from the above-mentioned fMRI and MEG study and the same stimuli in a new MEG experiment designed to study the source of response variability and hence to recognize the contribution of each of the major sources to this variability at the level of individual responses. The main objective of our work was to identify and characterize possible systematic processes governing the response generation, which are hidden behind the seemingly random fluctuations dominating the single-trial multichannel signal. To achieve this goal we analyzed the recorded data following three sequentially linked stages, starting with the MEG signal and continuing with the corresponding estimates of brain activity obtained from the tomographic analysis of this signal. First, we used a data-driven dimensionality reduction technique to derive a temporal signature corresponding to the activity of N70m generators, for each single-trial (ST). The extracted ST time courses were then handled using pattern analysis principles. The backbone of the overall methodology was the efficient design and application of an *encoder* that could summarize the variability of N70m responses. A vector quantization (VQ) scheme partitioned the data into groups and representative prototypes were computed. Based on these prototypes and by means of signal-processing and graph-theoretic techniques, the response variability was presented in an organized and intelligible way that provided insights into the mechanisms controlling it. Next, we used the estimates of brain activity to identify the consistent focal generators contributing to the prototypes formed in the first stage. Finally, the single-trial tomographic estimates were used to quantify the covariation of the activity in the primary visual area with the dominant signal pattern.

Materials and methods

Subjects and stimuli

Two subjects (S1 and S2, ages 27 and 25) volunteered for this study. Both of them had also participated in the previous fMRI and MEG experiment to examine the tomographic localization of activity within human V1 using whole-head MEG and 4-Telsa fMRI (Moradi et al., 2003).

The new MEG experiment was slightly modified. Identical stimuli were delivered, but, with higher luminosity than in the fMRI/MEG study in order to enhance the N70m response. The only other difference between the two experiments was the use of goggles at supine position in the first experiment and the use of brighter screen presentation at seated position in the new experiment. The procedure and scientific background for the experiment were fully explained to the subjects and signed agreement for participation was obtained prior to the experiment. Stimuli consisted of flickering (reversing) checkerboard patterns on a homogenous gray background: check size of 1°, 45° orientation, and 8° from a fixation point (a small red cross at the center of the screen) along the downward diagonal in one of the lower visual quadrants. The quadrant (left for S1 and right for S2) had been defined individually for each subject in the previous fMRI/MEG study to enhance the separation between V1 and the other areas and hence make V1 localization as unambiguous as possible. We used three checkerboard sizes (radii of 1.8°, 3.7°, and 4.5°) in three separate runs, which for ease of reference will be denoted hereafter as r18, r37, and r45, respectively. The reversal rate of the checkerboard was 1.43 Hz (i.e., each of the complementary patterns was presented for approximately 700 ms). The contrast of the stimulus was 93% (black 3 cd/m^2, white 85 cd/m^2, gray 44 cd/m^2). At a seated position, the subjects viewed the stimuli back-projected on a screen 56 cm from the subjects' eyes by an LCD projector outside the shielded room. A photodiode was attached to the screen to record the exact onset time of each pattern reversal. A separate subject baseline run served as control condition. This run had the same duration as the active runs and the subjects were scanned while fixating on the fixation point, but with no stimulus delivered in any quadrant. The gray screen background and the light background in the room were the same as in the active runs.

MEG signal recording and processing

The MEG signal was recorded with the 151-channel whole-head Omega biomagnetometer (CTF Systems Inc., Vancouver, B.C., Canada) inside a magnetically shielded room (NKK, Japan). Each MEG channel is a first-order axial gradiometer with two coils of 1 cm radius separated by 5 cm. Additional channels were used to monitor the subjects' artifacts resulting from blinks and vertical eye movements (EOG electrodes 1 cm above and below the left eye), horizontal eye movements (EOG electrodes 1 cm lateral to the left and right outer canthus of the eyes), and heart function (ECG electrodes, left and right wrists, left and right angles and lead V2). Before the MEG experiment, three head coils were attached to the subject's scalp, close to the nasion, and on the left and the right preauricular points. Three coils monitored the head position during the experiment for the definition of the coordinate system and the coregistration of MEG data with subject's MRI. The subjects sat in front of the centrally placed screen with the MEG helmet completely covering the whole head. During the MEG recording, the subjects were instructed to fixate on the fixation point and to stay alert. Before and after each recording run, the subject's head position was monitored. If the subject had moved excessively during a run (3 mm or more), that run was repeated.

The MEG signal was recorded continuously for each run with a sampling rate of 625 Hz after low pass filtering at 200 Hz. Each run consisted of 240 trials of pattern reversal and started with the presentation of the gray screen with the fixation point for 30 s. Environmental noise was first eliminated by forming the third gradient of the magnetic field off-line and the resulting data were further band-pass filtered in the 1–120 Hz range with notch filters at 50 and 100 Hz. The interference from the cardiac activity was then eliminated, utilizing the recorded ECG signals, via a noise cancellation technique based on linear regression (CTF software). Trials were extracted in the range from −100 to 200 ms relative to the onset of each pattern reversal. Trials with blinks or eye movements (changes greater than 50 μV in the EOG channels) were automatically removed. The exclusion of artifact-contaminated trials was further accomplished manually. On average, about 20% of the trials were removed. The number of the remaining trials available for single trial analysis is listed in Table 1. The procedure for extracting and selecting trials from the control condition run was the same as the procedure for the stimulation runs.

Virtual sensor transform

At the first stage, our analysis focused on a single time course signal synthesized from the multichannel data, via the virtual sensor (VS) transform, in a way that amplified the contribution from the complex of generators, being responsible for the dominant N70m response. Summarizing this spatial filtering action, a detailed description of which can be found elsewhere (Liu et al., 1998), we denote the *i*th single-trial response (scalar) signal collected by the *l*th MEG sensor, with sampling frequency f_s, as

$$x_i^1(t), \quad i = 1, \ldots, N;$$

$$t = \ldots 1 \cdot T_s, 2 \cdot T_s, \ldots = -100\text{: } T_s\text{: } 200 \text{ ms};$$

$$T_s = \frac{1}{f_s} = \frac{1}{625} \text{ s}.$$

First the averaged response,

$$\vec{x^1}(t) = \frac{1}{N} \sum_{i=1}^{N} x_i^1(t), \quad l = 1, \ldots, 151, \tag{1}$$

was formed for the r45-run and the MEG sensors $l_+(l_-)$ showing the most prominent positive (negative) deflection were identified and used to form the spatial filter

Table 1
Distribution of N70m-segments in the different groups

N_j (P value)	Group order										N	nDist.
	1	2	3	4	5	6	7	8	9	10		
S1												
Control condition	18.4	59.9	42	5.1	24.6	13.8	4.6	4	2.8	0.8	176	0.161
r18	13	51	31 ↓ 0.04	8	33	25 ↑ 9.e-07	5	7	5	4 ↑ 0.03	182	0.178
r37	12	38	37	14 ↑ 3e-11	29	15	4	10 ↑ 3e-04	6	3	168	0.181
r45	10 ↓ 0.04	21 ↓ 1e-08	20 ↓ 2e-04	26 ↑ <1e-12	35	24 ↑ 3e-06	12 ↑ 5e-04	12 ↑ 9e-06	8 ↑ 7e-03	10 ↑ 3e-11	178	0.152
S2												
Control condiction	0.125	9.5	49.5	16.25	33.75	18	9.75	2.75	3.625	0.75	144	0.242
r18	3 ↑ 3.e-08	16	4 ↓ 0.01	30	45	21	19	8	13 ↑ 0.002	3	207	0.220
r37	1	28 ↑ 6e-11	49 ↓ 0.01	36	28 ↓ 0.03	18	22	14 ↑ 0.002	8	3	207	0.230
r45	3 ↑ 5.e-09	28 ↑ 6e-07	42 ↓ 0.002	28	14 ↓ 4.e-04	11	27	18 ↑ 4.e-06	14 ↑ 2.e-04	12 ↑ <le-12	197	0.195

Note. The groups with a significant increase (decrease) in their population, at $P < 0.05$, are denoted using upward (downward) arrows, while the exact P value is tabulated.

$$x^{\mathrm{VS}}(t) = \frac{1}{5}\sum_{l_+=1}^{5} x^{l_+}(t) - \frac{1}{5}\sum_{l_-=1}^{5} x^{l_-}(t), \tag{2}$$

where $x^{l+}(t)$ and $x^{l-}(t)$ denote the signals from these sensors which were included, as shown in Fig. 1, in the dominant bipolar spatial pattern formed by the averaged multichannel signal in the early poststimulus period. The above spatial operator was then applied to the single-trial data to extract the signal $x_i(t)$, which for simplicity will be denoted hereafter with the superscript VS omitted. The time course defined by $x_i(t)$ was the signature of regional dynamics used to characterize, at the level of individual responses and under all the recording conditions, the behavior of the dominant generators of N70m brain wave.

Measures of stimulus-induced changes

We used two simple descriptors to characterize the process underlying the generation of the evoked response based on a set of N single-trials $x_i(t)$. The definition of these descriptors was in full accordance with the pattern-analytic approach we adopted in this study and motivated by previous work on single-trial analysis (Laskaris and Ioannides, 2001, 2002). The first descriptor is related to the concept of amplitude-modulation of a signal, while the second one is related to phase-modulation (Penny et al., 2002). Both descriptors were employed via a sliding window of p samples width. At every latency t, the single-trial segments

$$X_i(t,p) = \left[x_i\left(\mathrm{t} - \frac{p-1}{2}.T_s\right), \ldots, x_i(t - 1.T_s), x_i(t), \right.$$
$$\left. x_i(t + 1.T_s), \ldots, x_i\left(t + \frac{p-1}{2}.T_s\right) \right],$$
$$i = 1, 2, \ldots, N$$

were extracted and used in the computation of the time-varying energy (tv_Energy)

$$\mathrm{tv\_Energy}(t,p) = \frac{1}{N\,p}\sum_{i=1}^{N} \|X_i(t,p)\|^2 \tag{3}$$

and in the computation of a factor expressing the intertrial synchronization (ITS)

$$\mathrm{ITS}(t,p) = \frac{1}{N(N-1)}\sum_{i=1}^{N}\sum_{r\neq i}^{N} \left\| \frac{X_i(t,\,p)}{\|X_i(t,\,p)\|} - \frac{X_r(t,\,p)}{\|X_r(t,\,p)\|} \right\|^2. \tag{4}$$

The time course of these two descriptors can contribute to the understanding of the averaged response formation by

Fig. 1. A data-driven approach is followed for both constructing the spatial filter that extracts the time course of the visual evoked response and selecting the chain of samples that will be used to characterize the N70m brain wave. The data from the r45-run, where the stimulus shown in (a) was presented, are averaged. The dominant response in the early poststimulus period is identified and the emerged bipolar pattern leads to the selection of channels participating in the Virtual Sensor transform (b). Using the averaged VS-based signal from this run, a N70m-related latency range is defined via thresholding at zero-level, around the peak of the prominent deflection (c).

Fig. 2. Comparison of the averaged N70m response across the different recording conditions. The VS-based single-trials have been used to compute, for each run separately: (a) the average time course of the evoked response, (b) an estimate of the response signal-energy time course, and (c) an estimate of the intertrial synchronization time course.

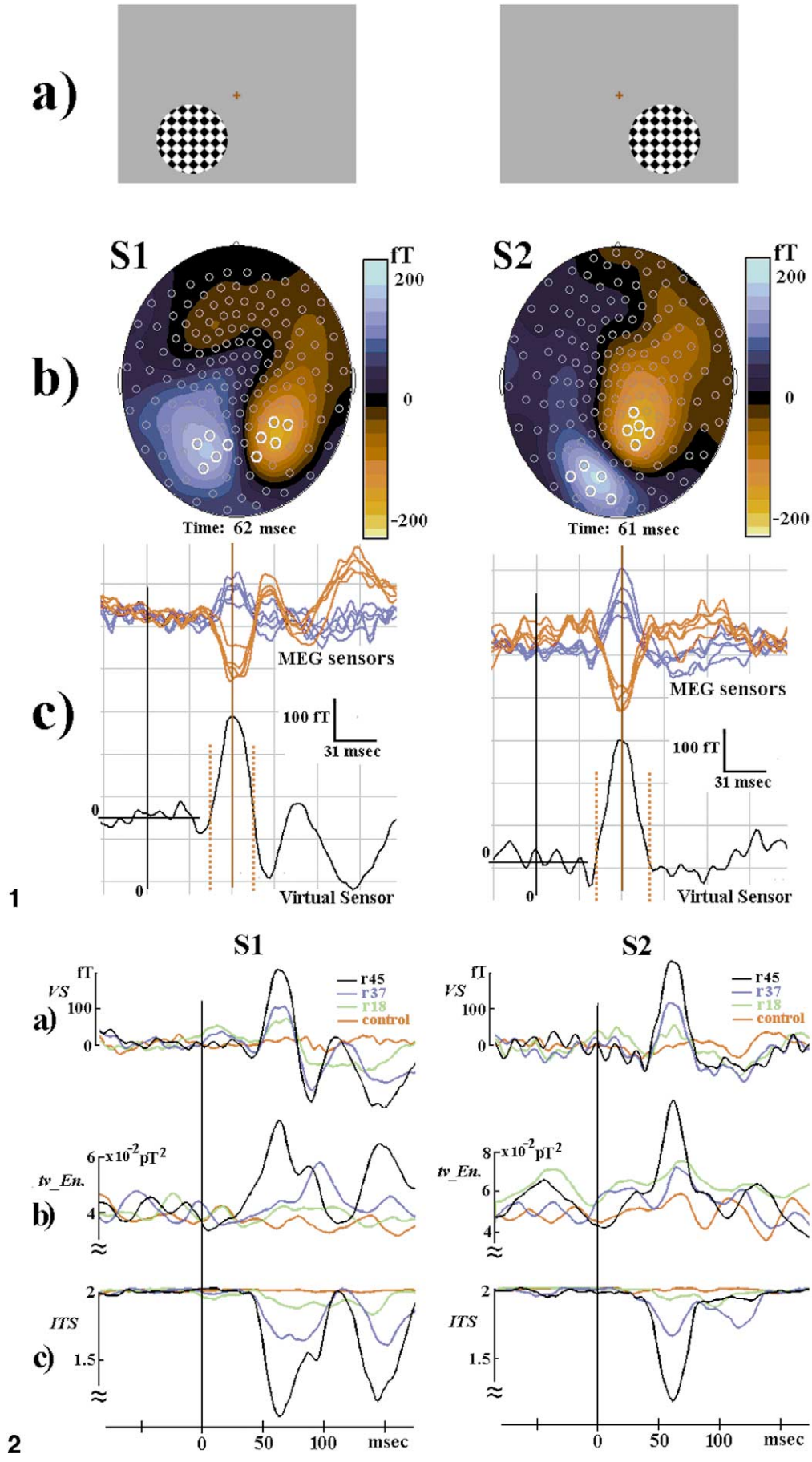
a)
b)
S1
S2
fT
200
0
-200
Time: 62 msec
Time: 61 msec
c)
MEG sensors
100 fT
31 msec
Virtual Sensor
1
S1
S2
VS
fT
100
0
r45
r37
r18
control
a)
tv_En.
x10^-2 pT^2
6
4
8
b)
ITS
2
1.5
c)
0
50
100
msec
2

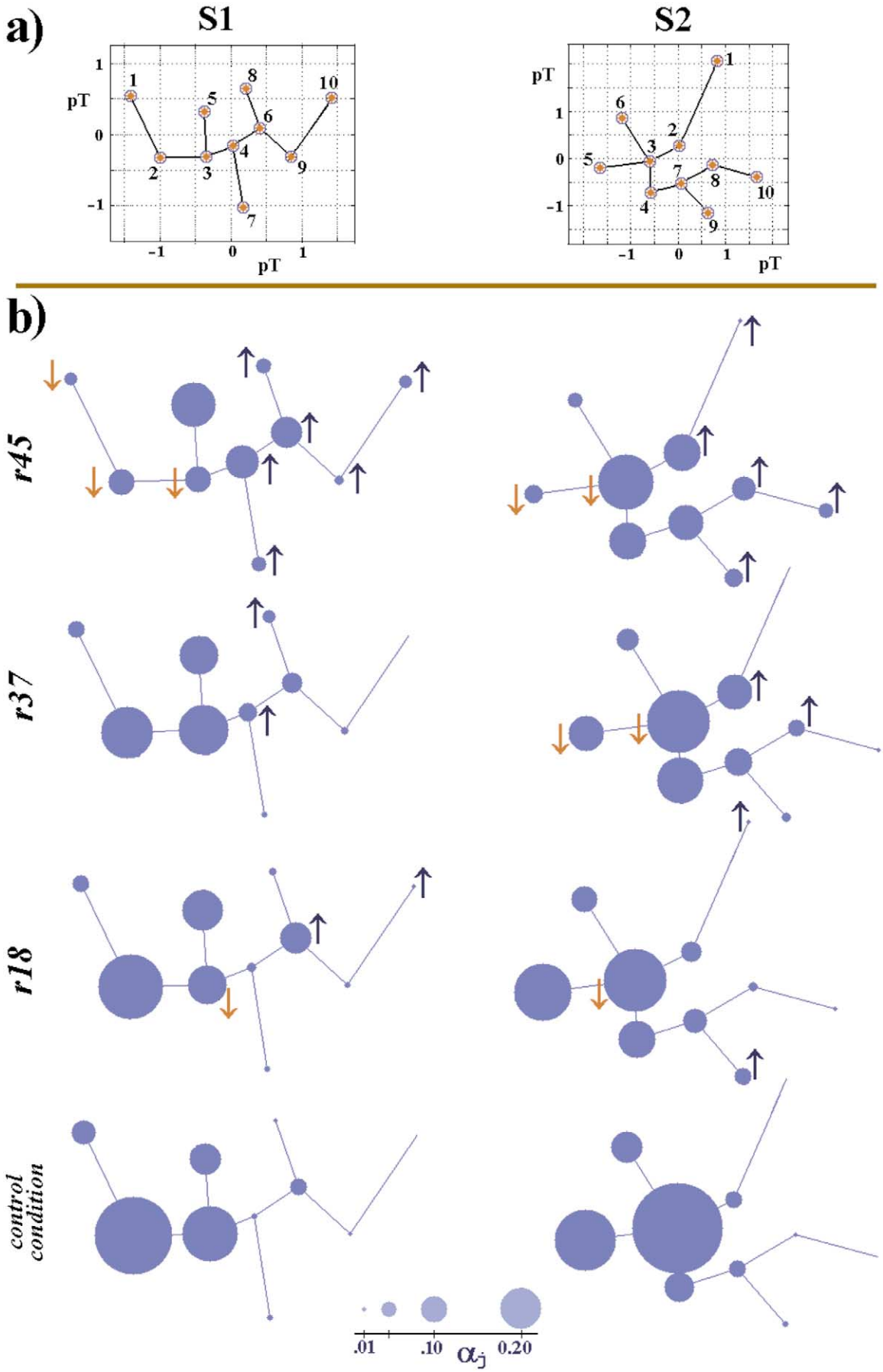
a)
S1
S2
pT
pT
b)
r45
r37
r18
control condition
.01
.10
α_j
0.20

revealing the role of the stimulus-induced changes in the ongoing activity. The former descriptor is associated with amplitude dynamics and can be used to mark loosely phase-locked increases or decreases in the strength of ongoing oscillations. The latter one is associated with phase dynamics and is closely related to both the phase-locking factor (Tallon-Baudry et al., 1996) and the event-related intertrial coherence (Makeig et al., 2002). In Eq.(4), a shape-dissimilarity measure is employed for performing all the pairwise comparisons between the ST-segments, which are then summarized by means of averaging. The range of values for the resulting ITS index is [0,4]. The zero value corresponds to the perfect alignment across trials while the value of two corresponds to a random one. A rapid drop in the time course of this index, while the tv_Energy(t) is remaining constant, indicates a well time-locked phase-reorganization event.

Pattern analysis of VS-based ST-signals

Feature extraction

The ensemble of $x_i(t)$, $i = 1, 2. . ., N$ signals from each run was treated as a collection of temporal patterns and pattern analysis principles were then employed for a detailed study of the N70m response variability. A simple data-driven procedure was adopted for extracting features from each ST-pattern (of all runs). Based on the pattern of the r45-run ensemble average, a set of p latencies around the latency $t_{\max}$ of the N70m peak was defined from the zero crossings around it (see Fig. 1). The chain of signal values at these latencies (i.e., the specific segment) constituted the set of extracted features. In this way, the feature vector extracted from the ith ST-pattern $x_i(t)$ was a p-dimensional vector of the form:

$$X_i = X_i(t_{\max}, p) = \left[x_i\left(t_{\max} - \frac{p-1}{2}.T_s \right), \ldots, \right.$$
$$x_i(t_{\max} - 1.T_s),\ x_i(t_{\max}),\ x_i(t_{\max} + 1.T_s), \ldots,$$
$$\left. x_i\left(t_{\max} + \frac{p-1}{2}.T_s \right) \right].$$

After the feature extraction step, the given record of N70m responses was treated as a collection of points embedded in a multidimensional feature space $\subseteq \mathbf{R^p}$. The ST segments were tabulated separately for each run in a corresponding (Nxp) data-matrix

$$\mathbf{X^{data}} = \mathbf{X^{data}}(t_{\max}, p) = [X_1|X_2|. . .|X_N],$$

that can be thought of as containing the different snapshots of regional brain activity during the specific poststimulus time interval.

Vector quantization

In short, vector quantization (VQ) techniques encode a data manifold $\mathbf{V} \subseteq \mathbf{R^p}$ utilizing only a finite set of reference or "codebook" vectors $O_j \in \mathbf{R^p}$, $j = 1, . . ., k$. A data vector $X \in \mathbf{V}$ is described by the best-matching or "winning" reference vector O_j, for which the distortion error is minimal. This procedure divides the manifold $\mathbf{V}$ into a number of subregions

$$\mathbf{V_i} = \{X \in \mathbf{V}: \|X - O_i\| \leq \|X - O_j\|\ \forall\ j\}$$

called Voronoi regions (or polygons), out of which each vector X is described by the corresponding reference vector O_i. The VQ procedure is the multidimensional analog of splitting a set of scalar values into bins of unequal, adaptively defined bin widths. It actually performs a parcellation of the Feature-Space, known as Voronoi Tessellation (Martinez and Schulten, 1994). The efficient application of VQ depends mainly on the proper selection of the reference vectors.

In this study VQ was invoked as a means of summarizing the information contained within each ensemble $\mathbf{X^{data}}$ of N70m snapshots, while inducing minimal distortion. The design of the encoder consisted of applying the "neural-gas" algorithm to the data matrix from the r45-run in order to compute the reference vectors. This algorithm is a neural network model (Choy and Siu, 1998; Atukorale and Suganthan, 2000), which converges efficiently to a small, user-defined number $k < N$ of codebook vectors, using a stochastic gradient descent procedure with a "soft-max" adaptation rule that minimizes the average distortion error. The computation of the k codebook vectors was followed by the application of the encoder: the nearest codebook vector was assigned to each X_i in the data matrix $\mathbf{X^{data}}$ for every run. This resulted in the k-partition of the corresponding ST-segments set, which was finally represented by an (Nxk) partition matrix **U,** with elements u_{ij} such that

$$u_{ij} = \begin{cases} 1 & \text{if } X_i \in V_j \\ 0 & \text{if } X_i \notin V_j \end{cases}, \sum_{j}^{k} \sum_{i=1}^{N} u_{ij} = N. \quad (5)$$

With this encoding scheme, the bulk of information con-

Fig. 3. A picturesque representation of the vector quantization results. (a) A 2D representation of the employed codebook is given, based on the MST graph of the included reference vectors. Each node corresponds to one reference vector and nearby nodes correspond to similar reference vectors. The index attached to each node has resulted from the graph-theoretic ordering of the reference vectors. This ordering enables the handling of the codebook in the form of an ordered list of reference vectors. The depicted ranks of the reference vectors also define the ranking of the corresponding Voronoi regions. (b) The tree diagrams shown have been based on the codebook vectors cartography given in a and graphically depict the distribution of the N70m single-trial segments in the different Voronoi regions, for each run separately. The blue (red) arrows indicate Voronoi regions with significant increase (decrease) in the proportion of N70m segments, which were more similar to the corresponding reference vectors. Because the significance has been assessed with respect to the distribution in the control condition run, this figure visualizes the effect of stimulation as a function of stimulus size.

tained in the data matrix was represented in a parsimonious way. The fidelity of the encoder was quantified via the following index, which is the total distortion error divided by the total dispersion of the data:

$$\bar{X} = \frac{1}{N}\sum_{i=1}^{N} X_i, \quad n\text{Distortion} = \frac{\sum_{i=1}^{N} u_{ij}\|X_i - O_j\|^2}{\sum_{i=1}^{N}\|X_i - \bar{X}\|^2}. \tag{6}$$

We tested the hypothesis that the stimulus induces changes in the population of the Voronoi regions. In order to assess the statistical significance of such a tendency, the VQ procedure was applied repeatedly to collections of ST segments sampled randomly from the control condition run dataset. The corresponding proportions of segments in each Voronoi region were calculated and used to form a baseline distribution for each region separately. Based on this baseline distribution, the deviation of the segments' proportion under each of the three stimulation conditions was expressed as a P value.

Visualizing the VQ results via tree diagrams

For ease in the presentation of the VQ results and to advance their interpretability, the Minimal Spanning Tree (MST) of the reference vectors was constructed (Kangas et al., 1990) and used in three ways: (1) to produce a two-dimensional map in which the reference vectors were represented as points and the relative morphological differences between these vectors were represented geometrically as interpoint distances, using a distance preserving technique known as "planing" (Laskaris and Ioannides, 2001); (2) to order them using a standard graph-theoretical procedure known as tree-diagram traversal (Laskaris and Ioannides, 2001; Baumgartner et al., 2001) (this ordering scheme provided an ordered list in which similar reference vectors have similar ranks and are used for the efficient handling of the single-trial data); (3) to visualize the distribution of ST segments in the different Voronoi regions, for each run separately, using the two-dimensional projection of the corresponding reference vectors and depicting graphically, with the size of MST nodes, the proportion of ST segments falling within each region.

Grouping ST patterns

The computed k partition was generalized from the ST segments $\{X_i\}_{i=1:N}$ to the corresponding ST patterns $x_i(t)$, $t = -100{:}200$ ms. The N_j patterns with segments assigned to the same Voronoi region $\mathbf{V}_j$ formed the jth group and a prototypical time course of regional brain activity was derived via within-group averaging. The computed subaverages $y_j(t)$, $j = 1, 2, \ldots, k$

$$N_j = \sum_{i=1}^{N} u_{ij}, \quad y_j(t) = \frac{\sum_{i=1}^{N} u_{ij}\, x_i(t)}{N_j} \tag{7}$$

represent the different modes of evoked response, collapsed into a single time course when ensemble averaging is applied. This can be expressed with the simple formula

$$\alpha_j = \frac{N_j}{N}, \quad \bar{x}(t) = \frac{1}{N}\sum_{i=1}^{N} x_i(t) = \sum_{j=1}^{k} \alpha_j\, y_j(t) \tag{8}$$

which shows, in mathematical terms, how the ensemble average can be decomposed into the above defined subaverages. In this decomposition, the mixing coefficient associated with the jth subaverage is the proportion α_j of the corresponding patterns assigned to the jth group. Such a decomposition is informative if the computed subaverages are different from each other, which is equivalent to the condition that the corresponding groups of ST patterns are forming compact, well-separated clusters (Fukunaga, 1990).

To validate the previous "forced clustering" procedure (Yager and Filev, 1994), a functional from the partitional-clustering literature (Jain and Dubes, 1988) was utilized. Using a moving window, the within-groups cohesion of the ST-patterns morphology was quantified as a function of latency. For every latency t, the endowed segments $\{X_i(t,p)\}_{i=1:N}$ were used to compute the total dispersion of the grouped patterns, which was then normalized by dividing it by the dispersion of the overall set of patterns as

$$n\text{Sc}(t) = \frac{\sum_{i=1}^{N}\sum_{j=1}^{k} u_{ij}\|X_i(t,\, p) - Y_j(t,\, p)\|^2}{\sum_{i=1}^{N}\|X_i(t,\, p) - \bar{X}(t,\, p)\|^2} \tag{9}$$

The resulting curve, denoted as $n\text{Sc}(t)$, expresses the reduction in the scattering of the ST patterns due to their partition into homogeneous groups and presents a value smaller than unity at the latencies where this partition is valid. A randomization test (Jain and Dubes, 1988) was employed independently for each set of segments corresponding to each latency, to assess the statistical significance of the obtained values.

Fig. 4. The ordered list of the prototypical N70m responses. The MST-based ordering of the reference vectors (Fig. 3a) defined the rank of each of the groups that the VS-based single-trial signals formed after the application of the vector quantization procedure to the data from the r45-run. The display of the computed within-group averages [Eq. (8)] has been organized according to the ranking of the corresponding groups. To emphasize the highly variable nature of the N70m response, all subaverages have been plotted using a common amplitude scale and are accompanied by the ensemble average (black thin trace). The number of single-trials that were included in the computation of each subaverage has been tabulated in Table 1.

Fig. 6. A Markovian analysis of the N70m response dynamics for the r45-run. (a) The state transition matrix (TM) which has been computed based on the sequence of response states as a function of stimulus repetition. (b) An estimate of the state transition matrix for the case that the within-run order of the single-trial responses was entirely random. (c) The most systematic transitions have been detected by thresholding the TM entries, at $P < 0.1$, based on a permutation test. An extra black frame denotes the transitions that were significant at $P < 0.01$ level.

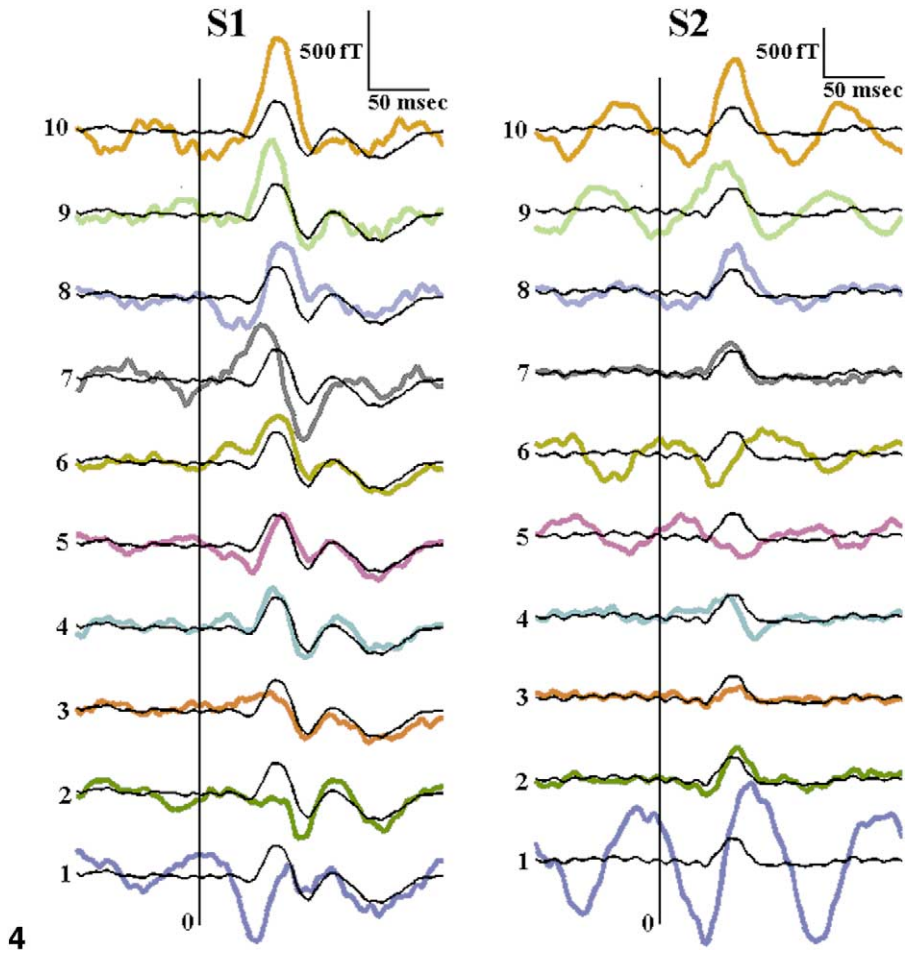
S1
500 fT
50 msec
S2
500 fT
50 msec
10
9
8
7
6
5
4
3
2
1
0

4

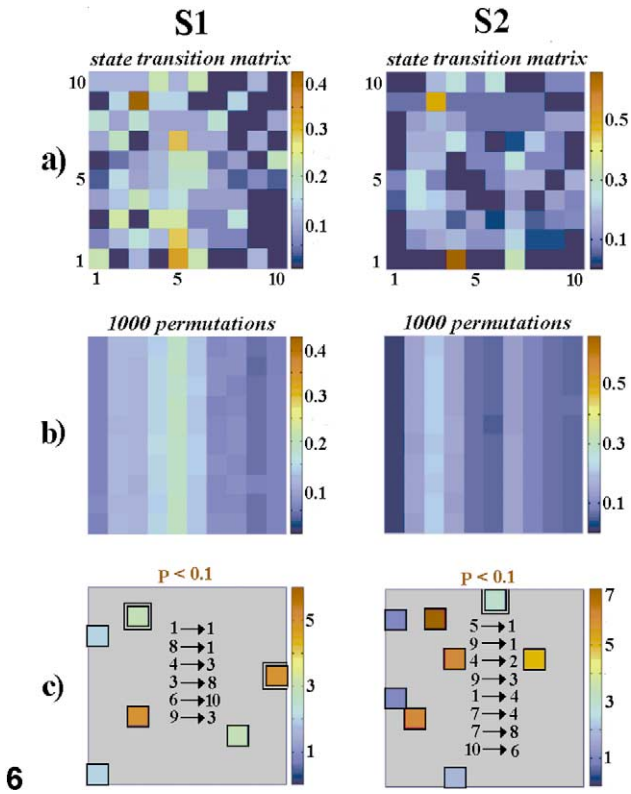
S1
S2
state transition matrix
state transition matrix
a)
b)
c)
1000 permutations
1000 permutations
P < 0.1
P < 0.1
1→1
8→1
4→3
3→8
6→10
9→3
5→1
9→1
4→2
9→3
1→4
7→4
7→8
10→6

6

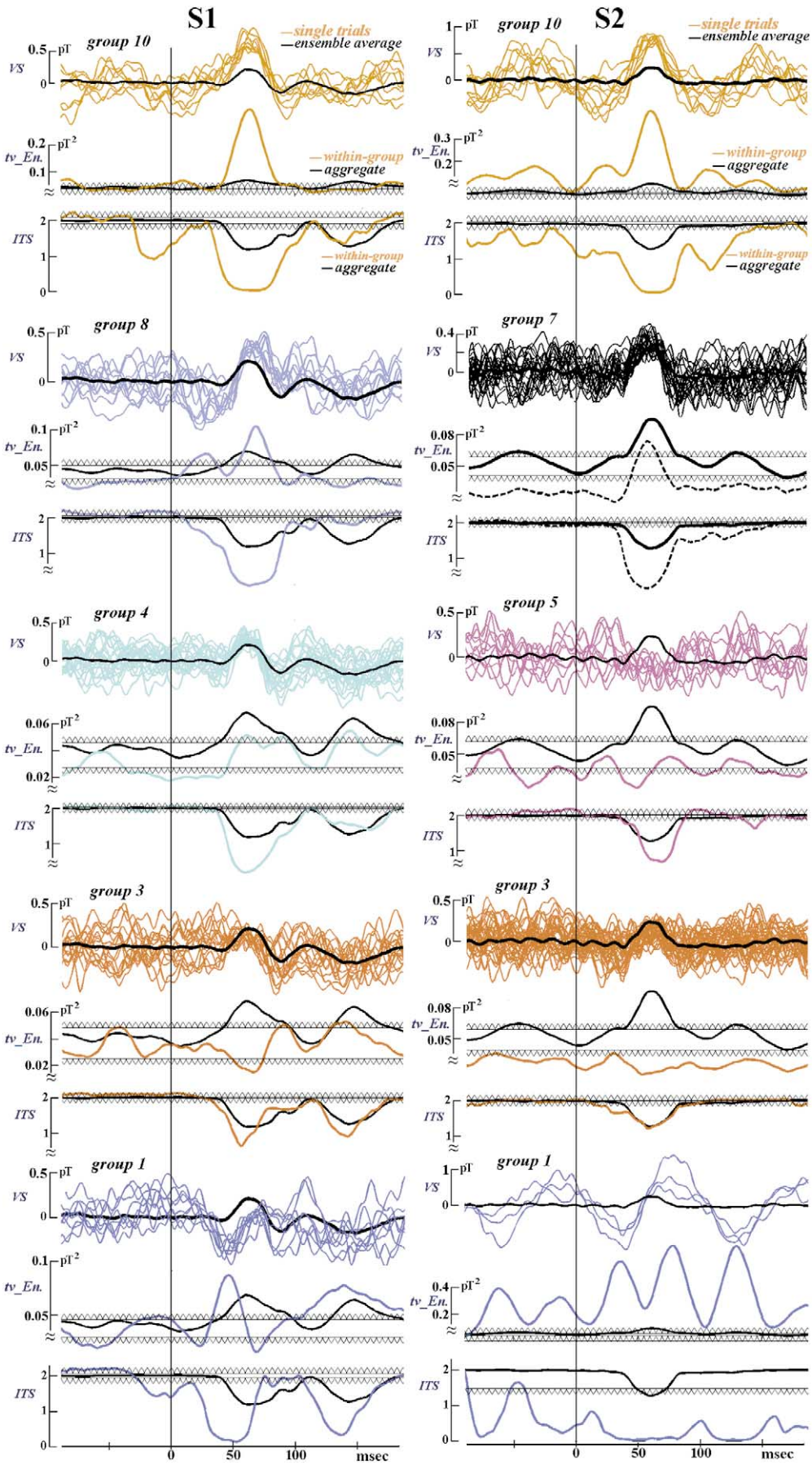
S1
S2
group 10
group 8
group 4
group 3
group 1
group 7
group 5
single trials
ensemble average
within-group
aggregate
VS
tv_En.
ITS
pT
pT²
msec
0
50
100

Within-group characterization of N70m evoked responses

The process underlying the generation of the evoked response was characterized for each group separately using the time-varying energy [Eq.(3)] and the intertrial synchronization [Eq.(4)]. The computations involved in the two descriptors were restricted among the single trials within each group. For instance, Eq.(3) took the form

$$tv\_\text{Energy}_j(t, p) = \frac{1}{N_j\, p} \sum_{i=1}^{N} u_{ij} \|X_i(t, p)\|^2, \quad j = 1{:}k. \tag{10}$$

In order to assess the statistical significance of the obtained measurements, the same procedure was applied repeatedly to samples of ST patterns, with exactly the same number N_j of curves, selected from the control condition run (via random sampling with replacement). The mean value and the standard deviation of the obtained measurements were subsequently estimated and used to signify the 99% confidence interval in the corresponding graphs. The adopted procedure provided us with the range of values that the *tv*_Energy (or the ITS) parameter can take when its estimation is based on data from the control condition. Fluctuations of the *tv*_Energy$_j(t)$ curve (or the ITS$_j(t)$ curve) outside this range can be considered as indications for stimulus-induced changes in the dynamics of brain activity and can characterize the *j*th group of responses.

Markovian analysis of evoked response succession

The variability of the N70m response within a run was studied further by adopting a Markovian approach, well fitted to the VQ-based encoding scheme. Following previous electroencephalographic studies, for instance (Jansen and Cheng, 1988; Ktonas et al., 2000), each Voronoi region V_i was treated as representing a specific state of the process generating the N70m response. For each run, the (*k*x*k*) transition matrix **TM** was computed from the sequence of N70m response states as a function of stimulus repetition. The *TM*(*i*,*j*) entry of this matrix indicated the probability that the process would go from state V_i (at the current trial) to state V_j (in the next stimulus application) and it was estimated using the formula

$$TM(i, j) = n_{v_i \to v_j} \cdot \Big(\sum_{j=1}^{k} n_{v_i \to v_j}\Big)^{-1}, \tag{11}$$

where the first term denotes the number of times during the run under study that the process had been observed to go from state V_i directly to state V_j. The gaps, which had been induced in the sequence of trials due to the exclusion of artifact contaminated trials, were taken into consideration.

A permutation test (Good, 2000) was applied to detect which of these first-order transitions were more (or less) frequent than in the case that the order with which the single trials had been recorded was of no importance. The N70m ST segments were reordered 1000 times (i.e., trial shuffling) and the corresponding transition matrices were estimated. The computed values corresponding to each cell (*i*,*j*) were used to form a distribution based upon which the significance of each transition probability *TM*(*i*,*j*) was assessed independently from the other entries.

Tomographic analysis of MEG signal

In order to identify the sources contributing to the signal emerged from the VS transform and relate their activity with the variability seen in the regional dynamics, we performed tomographic analysis of the MEG signal. Magnetic field tomography (MFT) (Ioannides et al., 1990; Ioannides, 1994) was applied to obtain tomographic localization of activity throughout the brain from the single-trial MEG data. MFT produced probabilistic estimates for the nonsilent primary current density vector **J**(**r,** *t*) at every time slice (1.6 ms) and for all the trials in a run. The single-trial MFT solutions were then grouped and subaveraged according to the *k* partition of the VS-based temporal patterns. This gave rise to prototypes of spatiotemporal maps of brain activity. Visual exploration of these MFT-based prototypes was performed within the broad region of sensitivity of the VS transform to identify the major generators of the N70m response and its variability.

Associating regional with local dynamics

We interpret the responses derived from the VS as regional, because the VS sensitivity, although considerably more restricted than that of the individual sensors, is still rather extended, covering a fairly wider area than say a cytoarchitectonically defined area like V1. Our experimental design allowed us to contrast these regional responses with local responses. Specifically we confirmed that the V1 location obtained in the earlier combined fMRI/MEG study (with stimuli placed in the same location in the visual field (Moradi et al., 2003)) was again activated in the new experiment. The exact location of V1, already identified from

Fig. 5. Characterizing the different modes of evoked response. Based on the MST diagram of Fig. 3a, five groups of VS-based single-trial signals have been selected and plotted using the same color with the corresponding prototypical responses shown in Fig. 4. Below the single-trial traces, and using the same color, the *tv*_Energy$_j(t)$ and the ITS$_j(t)$ traces are depicted providing a within-group characterization of the response dynamics. To ease the comparisons across groups, the ensemble average and the trace of the aggregate *tv*_Energy (ITS) for the r45-run have been superimposed (as black thick traces) to each group of trials and each within-group *tv*_Energy$_j$(ITS$_j$) trace accordingly.

the earlier study, was utilized to extract from the obtained single-trial MFT solutions, at the level of individual responses, a signature of the local dynamics. A region of interest (ROI) was first defined as a sphere with radius of 1.0 cm containing V1. For the *i*th single trial, an ROI activation curve (acv curve) $x_i^{\mathrm{ROI}}(t) = J_l^i(t)$ was then calculated along the main direction of the current density as a function of time, where $J_l^i(t) = \int_{\mathrm{ROI}} \mathbf{J}(\mathbf{r},t) \cdot \hat{\mathbf{u}}_{\mathrm{ROI}}\, d^3\mathbf{r}$ and with $\hat{\mathbf{u}}_{\mathrm{ROI}}$ representing the direction of the current density vector at the maximum (modulus) of the averaged MFT solutions within the ROI. For each run, the acv curves $x_i^{\mathrm{ROI}}(\mathbf{t})$, $i = 1, 2, \ldots N$ formed a new set of temporal patterns. A comparative study of this set and the corresponding set of VS-based ST patterns was carried out to associate the local with the regional dynamics, and hence investigate functional relationship between the regional and local neuronal responses.

We followed a structural association approach. The basic underlying principle in this approach is that the functional coupling of two brain areas can be detected as similarity, in terms of structure, between the two corresponding, concurrently recorded sets of single-trial signals (Laskaris and Ioannides, 2002). Specifically, to examine the possibility that the regional dynamics might affect the generation of response in the early visual areas, we compared the structure detected in the ensemble of N70m snapshots from a run (as expressed by the elements u_{ij} of the partition matrix **U** [Eq. (5)], with the structure in the corresponding set of single-trial acv curves from the V1-related ROI. To this end, we grouped the acv curves according to the partition matrix **U** and performed within-group averaging. The resulted subaverages

$$N_j = \sum_{i=1}^{N} u_{ij}, \quad y_j^{\mathrm{ROI}}(t) = \frac{\sum_{i=1}^{N} u_{ij} x_j^{\mathrm{ROI}}(t)}{N_j}, \qquad j=1, 2, \ldots, k \quad (12)$$

were compared with each other. The latency ranges, where these curves become more dissimilar (or equivalently the corresponding groups of acv curves were forming homogeneous clusters), corresponded to events of functional dependence of the neural activity in the circumscribed ROI on the N70 response. To quantify such a trend in our data, we replaced in the definition of the nSc index [see Eq. (9)] the set $\{x_i(t)\}_{i=1:N}$ of VS-based patterns with the set $\{x_i^{\mathrm{ROI}}(t)\}_{i=1:N}$ of acv curves and used the resulting index to validate the grouping of the acv curves. In this case, the nSc index served as a nonlinear interdependence measure, which quantified the functional covariation of regional and local activity. The obtained *n*Sc(*t*) curve can be thought of as a "transfer function" showing if/how the structure detected in the set of N70 snapshots manifests itself in the set of single trials from the lower-order visual areas.

Results

A regional study of the evoked response variability

The averaged (VS-based) evoked response

In both subjects, the averaged multichannel signal from the r45-run showed a very clear early evoked response. The spatial bipolar pattern at the denoted latency (Fig. 1b) guided the selection of the channels used in the VS transform [Eq.(2)]. The VS signal shown in Fig. 1c (black trace) reflects the temporal evolution of the averaged N70m response, which appears as a clear deflection from a zero baseline.

After applying the designed VS operator to the single-trial data under all the conditions, the extracted ST patterns were averaged for each run separately. Fig. 2 contains the comparison of the averaged N70m response across the different runs. The averaged signals are superimposed in Fig. 2a, while in Fig. 2b and c the *t*v_Energy(*t*) curve and the ITS(t) curve are given in the same format, providing an aggregate characterization of the response generation in the different runs. Taking into consideration the traces of both descriptors across runs, two facts, often overlooked when dealing with averaged data, are revealed. First, despite the zero baseline seen in the average response, a continuously active system is stimulated. Second, despite the gradual alteration of the averaged N70m deflection with the stimulus size, the mode of the evoked response actually switches in a nonlinear fashion. The averaged N70m response in the r45-run is built mainly via a time-locked increase of the poststimulus activity relative to the activity in the prestimulus interval. On the contrary, the phase reorganization of the

Fig. 7. Activation in polymodal parietal areas (BA5/7) obtained from the single-trial MFT solutions around the latency of N70m response. The instantaneous maps of current density vectors at three latencies for the five prototypes described in Fig. 5 for subjects S1 and S2 are shown on the left and right panels, respectively. Each map is displayed at a midsagittal slice through the identified BA5/7 area. Each row corresponds to one prototype. The normalization for each map has been done separately, but in order to ease comparisons, the maximum current density within each map is printed in text at the top of each map as a fraction of the overall maximum appearing in one of the 15 maps. The green outline denotes the sensitivity profile of the VS for subject S1 at level 0.3 and for subject S2 at level 0.1.

Fig. 9. Validation of the *k*-partition emerged by the application of the VQ-based procedure to the set of N70m single-trial snapshots from the r45-run. The indices assigning the N70m segments to different Voronoi regions were used to split into groups both the set of VS-based single trials (reflecting regional dynamics) and the set of the corresponding signals from the ROI containing the early visual areas (reflecting local dynamics). The top panel shows the latency-dependent normalized dispersion of the grouped VS-based single-trial patterns, while the bottom panel shows the corresponding trace computed for the within V1-ROI single-trial activation curves. The N70m-related latency range, based on which the k-partition was computed, is depicted using a gray shade.

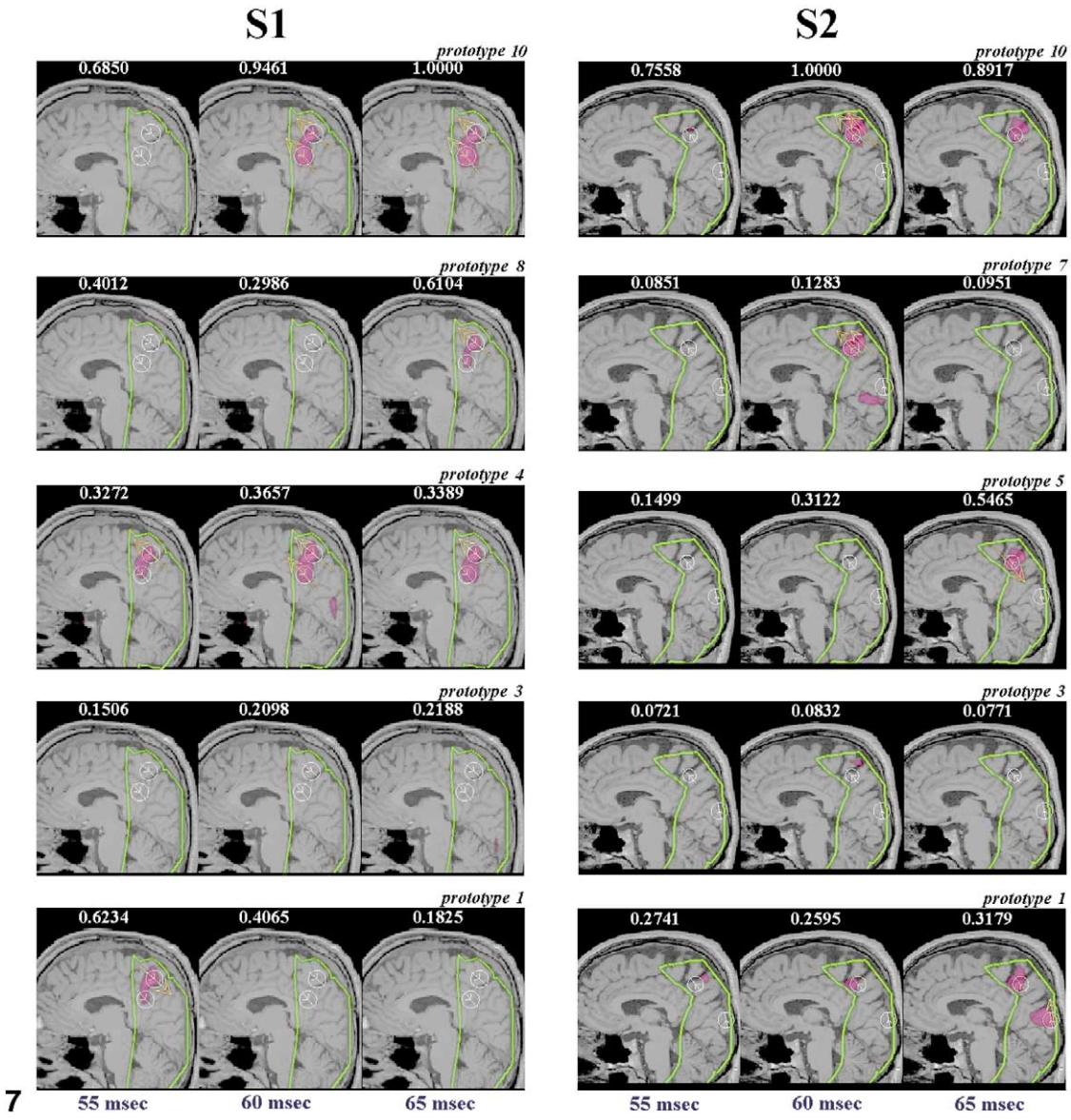
S1
S2
prototype 10
0.6850
0.9461
1.0000
0.7558
1.0000
0.8917
prototype 8
0.4012
0.2986
0.6104
prototype 7
0.0851
0.1283
0.0951
prototype 4
0.3272
0.3657
0.3389
prototype 5
0.1499
0.3122
0.5465
prototype 3
0.1506
0.2098
0.2188
prototype 3
0.0721
0.0832
0.0771
prototype 1
0.6234
0.4065
0.1825
prototype 1
0.2741
0.2595
0.3179
55 msec
60 msec
65 msec
55 msec
60 msec
65 msec

7

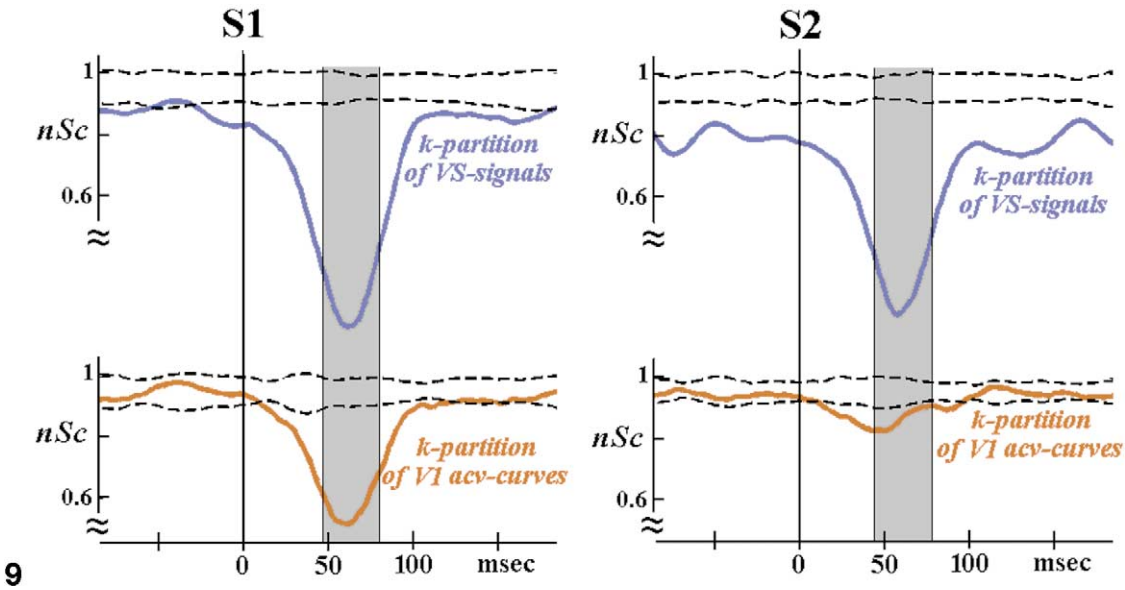
S1
S2
1
nSc
0.6
k-partition
of VS-signals
k-partition
of V1 acv-curves
0
50
100
msec

9

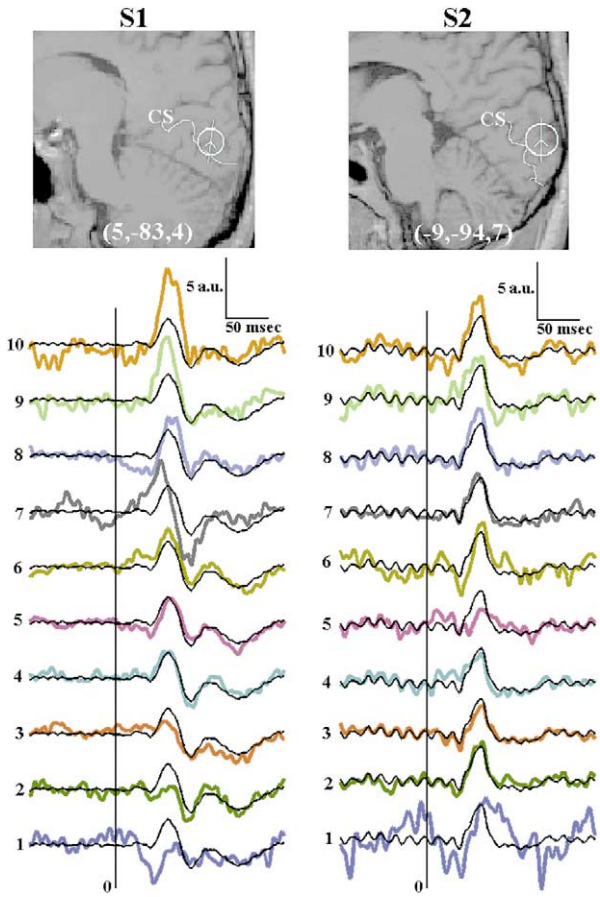

Fig. 8. Organizing the responses from the primary visual cortex (V1) based on the ordered structure of N70m variability. Top panel: for each subject, the V1 related ROI is plotted as a white circle with a white arrow indicating the main direction of the current density vector from the MFT solutions. The Talaraich coordinates for the V1 ROI are also printed in text (*x, y, z:* mm) and the calcarine sulcus (CS) is highlighted as a white curve. Bottom panel: the within-ROI single-trial activation curves have been grouped according to the *k*-partition of the VS-based single trials and the prototypical courses of activation, computed via within-group averaging [Eq. (12)], are presented in a form of ordered list that corresponds to the one presented in Fig. 4. The subaverages have been plotted using a common amplitude scale and are accompanied by the ensemble average of the activation curves (black thin trace).

ongoing activity contributes mostly to the formation of the averaged-N70m response in the r18-run.

A VQ-based study of the N70m variability

Based on the single-trials segments from the r45-run, which was the run corresponding to the strongest average N70m response (see Fig. 2), an encoder of $k = 10$ reference vectors was designed. The computed reference vectors were then ranked utilizing their MST graph (see Fig. 3, top) and this ranking defined the labeling $j = 1{:}10$ of the corresponding Voronoi regions V_j subsequently used in the VQ procedure, which was applied to each set of N70m-related segments from all runs. The adopted encoding scheme was validated for each run separately using Eq.(6). The computed nDistortion index, in all cases, was found to be $\ll 1$ (see Table 1, last column). This showed that the set of reference vectors computed from the r45-run could be used to represent the response variability in all the runs (or equivalently the Voronoi regions could be kept fixed across the different runs). This in turn allowed us to compare the results obtained by applying the VQ procedure to different runs. The number N_j of N70m segments falling in the jth Voronoi region has been tabulated in Table 1, where in the case of the control condition run an average estimate (see Methods) has been included. Fig. 3 is a pictorial representation of these results graphically depicting the corresponding proportions $a_j = N_j/N$. The Voronoi regions were populated in a stimulus-size-dependent manner. In both Table 1 and Fig. 3, the Voronoi regions with a significant increase (decrease) in this proportion, at level $P < 0.05$, have been denoted by upward (downward) arrows. It is evident when comparing the different runs that the increase in the stimulus size causes the shift of ST segments from some specific branches of the tree diagram to other branches (especially toward Voronoi regions S1: 4, 6, 7, 8, 9, 10 and S2: 2, 8, 9, 10). Fig. 3 clearly shows that the greater the visual stimulus size, the higher the response variability is, because it is the r45-run in which the N70m segments are distributed most uniformly.

The different prototypical (VS-based) evoked responses

The set of ST patterns from each run was split into $k = 10$ groups according to the assignment of the corresponding N70m segments to the predefined Voronoi regions. The labeling of these regions defined the labeling of the formed groups. This in turn enabled the orderly presentation of the prototypical evoked responses produced via within-group averaging [Eq. (7)]. Fig. 4 contains the N70m prototypes computed from the ST patterns of the r45 run in direct contrast with the ensemble average, which clearly indicates that the variability of the N70m response has both amplitude and latency facets. Despite the "transient character" of the averaged response, there are subaverages (S1:1,10 and S2: 1,5,6,10) showing that the single-trial activity may present oscillatory characteristics. The organized display of Fig. 4 clearly indicates that the prestimulus activity and the post-stimulus activity are strongly coupled, because the prototypical responses differ well before the selected latency range upon which the grouping was based. Two tendencies are worth noting. First, the amplitude of the (sub)averaged response is higher whenever the prestimulus oscillatory activity is characterized by high amplitude, supporting the hypothesis that the strength of evoked response depends on the amount of prestimulus α activity (Brandt et al., 1991; Makeig et al., 2002). Second, the phase of the ongoing oscillatory activity at the time of stimulus onset plays a critical role in the evolution of the evoked response (Jansen and Brandt, 1991), as can be inferred by contrasting two of the subaverages (for S1:1 vs 10 and for S2:6 vs 10). It should be noted that a high consistency was evident regarding the morphological characteristics of the obtained proto-

types, when the grouping procedure was repeated for the ST-pattern sets from the other runs.

The rich dynamic behavior of the N70m generators, as revealed by the grouping and subsequent subaveraging of the ST patterns, indicated the existence of distinct modes of evoked response that the application of ensemble averaging had compressed in one single waveform. VQ disentangled these modes and enabled a natural decomposition of the averaged signal in terms of the computed subaverages [see Eq. (8)], To examine if this decomposition, which had been optimized for the latencies around the N70m deflection, was meaningful in any other latency range, the $n\mathrm{Sc}(t)$ curve [Eq. (9)] was computed. For all the runs, the grouping of ST patterns was found to be valid not only within the N70m latency range, but also well before. This indicated that the structure seen in the set of N70m snapshots depended on the structure in sets corresponding to earlier single-trial segments.

Characterizing the different modes of response

To characterize the distinct evoked response modes associated with the different groups, the time courses of time-varying energy and the intertrial synchronization descriptors were computed for each group separately and contrasted with the corresponding ones computed for the overall set of ST waveforms in the run. Fig. 5 shows the results of this characterization for the case of five groups from the r45 run. The selection of these five groups was based on the MST graph of the 10 reference vectors used in the VQ procedure. Given that the reference vectors provided a compact description of the N70m-related dynamic manifold, their MST graph was considered as the skeleton of the response variability. Using the faithful representation of this graph given in the top panel of Fig. 3, five among the 10 reference vectors were selected to cover the whole range of dynamic behavior. The five groups of ST patterns associated with the selected reference vectors were the ones included in Fig. 5. The characterization of the rest of the groups can be "inferred" using the characterization of the groups corresponding to nearby MST nodes. For each of the selected groups, the N_j ST waveforms have been included in the top panel along with the overall average of the N waveforms which is shown in black. The time course of the within-group *tv*_Energy descriptor [Eq. (10)] has been included in the middle panel, while that of the within-group ITS descriptor is in the bottom panel. The horizontal lines depict the 99% confidence interval for the "null hypothesis" that the shown fluctuations of these parameters can be observed under control condition as well, and therefore they cannot be assigned to stimulus-induced perturbations. For comparison purposes, the $t\mathrm{v\_Energy}(t)$ curve and the $\mathrm{ITS}(t)$ curve corresponding to the overall set have been also included in the corresponding panels of Fig. 5 (as black thick lines). This graphical contrast of the different response dynamics clearly indicates that a highly adaptive system is stimulated. Distinct processes underlie the response generation in the different groups of single trials. The mode of response can change within a run from a transient increase in the signal energy of the activity to the phase resetting of the ongoing regional activity (compare the groups 3 and 10 of subject S1). Apart from these two well-known evoked response scenarios, the emergence of other modes is also observed. For instance, groups exist in which the included responses are better described as stimulus-induced enhancement of the ongoing rhythmic activity (S2: group 10 and especially group 1) or stimulus-induced desynchronization (S1: group 3). Interestingly, the group with subaverage similar to the ensemble average (for S1: group 4 and for S2: group 7) is characterized by a significantly low level of activity before the stimulus onset followed by a transient increase in the energy just after the onset. The particular mode can therefore be considered an entrainment of the N70m generators by the periodic stimulation.

The dynamics of N70m response succession

A Markovian approach was carried out to investigate possible underlying mechanisms that work at longer time scales and shape the N70m response generation by controlling the transition between successive responses. Fig. 6 contains such a characterization of the trial-to-trial dynamics for the r45 run. The computed state transition matrix TM (Fig. 6a) differs substantially from the transition matrix, which is given in Fig. 6b and corresponds to shuffled single trials (average over 1000 permutations). The image given in Fig. 6c shows the transitions that occurred systematically. Those entries which did not correspond to transitions more (or less) frequent than in the case of shuffled data (at $P < 0.1$ significance level) are shown in gray, and the rest of the entries are depicted using a coloring that denotes the absolute number of transitions. An extra black frame is used to denote a transition that was significant at $P < 0.01$ level. While a significant increase in the frequency of a few first-order transitions was detected indicating that the response succession was partially of deterministic character, no significant decrease was detected. The most striking result is that for both subjects, at $P < 0.01$ significance level, the transition from a high-responsiveness state to a low-responsiveness state (S1:9→3, S2:10→6) is revealed to be the most important law governing the sequence of responses. Similar results were also observed in the other stimulation runs, when the above thresholding scheme was applied using a higher significance level as threshold.

Associating the N70m response variability with the reconstructed brain activity

After grouping the single-trial MFT solutions based on the partition of the N70m snapshots, activations in widely separated areas were identified, for each group average. The MFT-related prototypes based on the N70m classification were dominated by contributions from polymodal parietal areas which appeared consistently in the different MFT

prototypes but at different latencies. The phase and strength of the activity in a near midline region on the border of BA5 and BA7 (for S1 (3, −40, 57) and for S2 (0, −46, 47) in talairach coordinates) best correlated with the patterns of the VS-based prototypes showing a strong N70m response. The V1 contribution to the N70m response and prototype formation was considerably weaker than the contribution from the polymodal areas. Fig. 7 shows the instantaneous maps of current density vectors at three different latencies for the five prototypes described in Fig. 5 at a midsagittal slice through the identified BA5/7 area. The triplet of maps corresponding to one prototype was normalized, originally, independently from the others. To enable comparisons across prototypes, the maximum current density within each map is given at the top of each map as a fraction of the overall maximum appearing in one of the 15 maps. The green outline shown in these maps denotes the sensitivity profile of the VS at level 0.3(0.1) for subject S1(S2). The white circles correspond to spherical ROIs that were defined over areas showing increased activity in the latency range around the N70m-peak latency. The topmost of them depicts the location of the BA5/7 area. The white arrow attached to each ROI indicates the direction of the current density vector at the maximum of the averaged MFT solutions within the ROI. The yellow arrows mark the positions of local maxima in the instantaneous maps and denote the corresponding directions of the current density vector. The regions corresponding to activity higher than the 60% of the maximum of brain activity within each triplet of maps have been colored purple. For subject S2, the displayed sagittal view contains the V1-related ROI (the bottommost circle), which shows activity at the given threshold only for one prototype, at about 20% of the overall maximal activity.

The N70m response variability and its relationship to the activity in primary visual cortex

To examine the possibility for a functional covariation of the regional activity reflected in the VS-based signals with the activity within the ROI containing V1 (Fig. 8, top), the *k* partition from each run was applied to the corresponding ROI single-trial activation curves and prototypes of local activity were computed [Eq. (12)]. The visual inspection of the computed prototypes was used to detect the structural similarity between the set of VS patterns and the set of ROI acv curves, which was further assessed using the nSC index.

Fig. 8 shows the local activity prototypes from the r45 run in exactly the same format as the corresponding VS-based ones given in Fig. 4. The comparison between Figs. 4 and 8 shows that the single-trial variability of N70m response as summarized by the VS-based prototypes has a functional counterpart in the ROI acv curves. As a quantitative measure of the strength of the observed functional covariation, the $n\mathrm{SC}(t)$ curve was computed expressing the validity of the VS-based grouping for the ROI activations. The bottom panel in Fig. 9 shows the latency dependence of the nSC parameter along with the 99% confidence interval of the corresponding null hypothesis that this grouping is a random partition. Fig. 9 shows that the *k* partition constitutes a valid description of the single trial variability around the N70m latency range for both the VS-based signals (from the N70m segments of which it has been computed) and the V1 related acv curves, which were derived independently from the single trial tomographic solutions. There are also differences in the latency range over which the *k* partition produces a significant reduction in the variance of the involved waveforms. For the V1 acv curves (Fig. 9, bottom) this latency range is confined to the poststimulus period from 10 to 100 ms, while for the VS-based time series (Fig. 9, top), it extends through almost the entire latency range, including the prestimulus and late poststimulus periods (the examined period was from −100 to 200 ms).

Discussion

The study of regional response dynamics

We studied the single trial variability in N70m visual responses in a novel way using pattern analysis principles combined with graph theoretic and signal analysis tools. The dominant spatial pattern in the averaged signal during the N70m latency range was used to define a simple spatial operator using sensors over the occipital and parietal areas. The virtual sensor (VS) transform was then applied to the multichannel data producing, for each single-trial response, a time series encapsulating the regional dynamics. The N70m response variability was then encoded via vector quantization in a simpler format by simply assigning the membership of each time series to one of the different response classes. The 10 reference vectors used in the adopted encoding scheme had been computed from the run presenting the highest N70m response variability in order to ensure no loss of information. An efficient neural computation algorithm, powerful in discovering potential self-organization tendencies in the N70m-related dynamic manifold (Penny et al., 2002), was employed for the definition of the reference vectors. The number *k* of reference vectors was set to 10, after extensive experimentation which showed no qualitative differences when *k* increased, as the best trade-off between a detailed encoding of variability and a convenient presentation of the subsequent results. Our analysis showed that it was possible to describe the broad spectrum of N70m responses by means of 10 principal modes, which summarized the variability seen in the MEG signal and further served as the starting point for exploring the source of that variability based on estimates of reconstructed brain activity.

Aggregate characterization of the evoked response

We have used two simple descriptors (time-varying energy, *tv*_Energy and intertrial synchronization, ITS) to obtain measures aggregated over an ensemble of single trials and characterizing the time course of response within a run. The comparisons between runs of different stimulus sizes (Fig. 2) have shown that, even with such a simple stimulation paradigm, a continuously active, nonlinear system is probed. The output (N70m response) is not a linear transform of the input (stimulus) as it appears to be when comparing the averaged signals from different runs. The averaged response is built, in the case of a big stimulus, mainly through a time-locked, relative increase of the poststimulus activity, while in the case of a small stimulus, through the phase reordering of the ongoing brain waves.

Grouping and within-group characterization of single trial responses

By splitting the ensemble of ST patterns into homogeneous groups and performing a within-group characterization of the evoked response, it has been shown that a variety of distinct response modes can appear within a single run. Each mode presents its own dynamical behavior that, in some cases, is influenced by ongoing activity well before the onset of the averaged N70m response. We have demonstrated that ongoing rhythmic activity before the onset of the stimulus is functionally coupled with the subsequent response. Both the phase and amplitude of this rhythmic activity at the time of stimulus determines the poststimulus response (Makeig et al., 2002). The existence of a set of responses (S1: group 4 and S2:group 7 in Fig. 5) during which the regional activity appears to be enslaved by the exerted periodic forcing indicates the adaptive nature of the ongoing rhythms. The overall spectrum of our results extends the current dichotomy between "stimulus-evoked time-locked brain events" and "stimulus-induced phase resetting of ongoing waves" to a variety of complex nonlinear interactions between the sensory input and the encephalographic processes.

The stimulus size controls the frequency of appearance of the different response modes within a run in a systematic way (Fig. 3). In addition, the process underlying the response transition from one mode to another is considerably different from a stochastic one (Fig. 6). These findings together with the fact that the characteristics of each response mode contain statistically significant stimulus-related events (Fig. 5), provide a strong indication that the variability seen in the VS signal reflects a polymorphic processing of the incoming stimuli and not random fluctuations.

Figs. 4 and 5 present the variability in the regional activity in an organized fashion clearly indicating that the single-trial traces in our data cannot be described by the "signal plus noise" model. Our results are consistent with a state-dependent response (Kisley and Gerstein, 1999; Lutz et al., 2002). The $n\mathrm{Sc}(t)$ index provides time-dependent quantification of the grouping quality, which shows, in a mathematically sound way, that the structure detected in the single-trial data within the latency range of N70m deflection depends strongly on the single-trial activity at earlier latencies (Fig. 9, top).

Distinct dynamics are fused into one time course by ensemble averaging

Ensemble averaging, by falsely treating the ongoing activity as being indifferent to the stimulus, suppresses in a single waveform entirely different modes of evoked response (Mast and Victor, 1991; Liu and Ioannides, 1996; Fries et al., 2001). Unless there is a predominant mode, the computed average is a mirage of the response generation process where different dynamics have been collapsed. The so-called "trial-to-trial nonstationarity" has been shown to lead, when is not taken into consideration, after averaging to erroneous interpretations regarding not only the time course of the response, but also the temporal modulation of measures like the power spectrum and the cross correlation (Truccolo et al., 2002), because an averaging step is also included in their estimation. This becomes directly evident also from our results, when the aggregate characterization of the response dynamics is compared with the corresponding within-group ones (Fig. 5). The introduced decomposition formula [Eq. (8)] models this effect for the ensemble averaging of the single trial signals. The same decomposition holds for every other set of time courses, which are first deduced for individual single trials and then averaged to produce an aggregate latency dependent measure like the *t*v_Energy trace [Eq. (3)]. Specifically, Eq. (8) can be invoked to offer an explanation for the change of averaged N70m response with the size of the stimulus (Fig. 2) within the framework of a "state-dependent response." It is the relative frequency with which the distinct response modes appear during a run that is altered with the increase of the stimulus size (see Fig. 3 and Table 1).

The source of N70m variability

The diversity of results regarding the nature of the early responses to simple visual stimuli, and especially the N70m response in earlier studies using averaged signals (Russo et al., 2001; Tzelepi et al., 2001; Vanni et al., 2001; Foxe and Simpson, 2002), is likely to be not only due to differences in experimental protocol and source reconstruction analysis, but also due to mixing distinct response histories and/or neglecting the active role played by the associated ongoing activity. The exploration of the MFT-based spatiotemporal counterparts of the VS-based prototypical responses has shown that among the widespread network of ongoing activity generators, the sources which contribute most to the variability in the signal properties of the N70m response

seen in the virtual signal correspond to multimodal areas, while the activity in the primary visual area has a relatively negligible contribution.

The coupling of primary visual area responses to the regional dynamics

Our results suggest that a prerequisite for the reliable characterization of the activity in the primary visual area is the sorting out of the dominant contributions coming in different modes from the polymodal areas. The structural coherence between the regional single-trial data and the contemporary ROI single-trial activation curves, expressed by the nSc(t) index (Fig. 9, bottom panel), demonstrates the functional covariation of regional and local responses. The latency range of significant nSc values for V1 is confined to a narrow range of latencies, consistent with a causal influence by the stimulus and the known timing of V1 activation. In contrast, the partition of VS signals leads to significant nSc values (Fig. 9, top panel) for a very extensive range of latencies, suggesting that the V1 response is also strongly conditioned by the activity in the multimodal areas, and hence a very strong and very early top-down influence on visual processing. Significantly, for both subjects, the nSc for the V1 partition precedes the corresponding minimum for the VS partition by a few milliseconds, suggesting a bottom-up influence. Therefore, the nature of the variability in the ROI activations indicates a close relationship between the ongoing rhythms and V1 activity, which cannot be fully encapsulated by a bottom-up vs top-down dichotomy. Our results are in accordance with the picture of a "temporally compact" visual cortex (Hupe et al., 2001).

Links with earlier studies

Our methodology is similar in principle to an approach employed recently for studying the evoked response variability in recordings of local-field potential and single-unity activity from the rat auditory cortex (Kisley and Gerstein, 1999). In that study, the single-trial traces were analyzed based on their waveforms using principal component analysis (PCA) in combination with a clustering procedure that is empirical in nature. The authors showed the failure of the "signal plus noise" model for their data, also, by identifying groups of responses which differed in both amplitude and shape. The response was found to be modulated by the preceding ongoing activity and the observed variability was attributed to rapid transitions between different levels of thalamocortical excitability.

In a more recent EEG study of single-trial variability (Lutz et al., 2002), the responses were grouped according to first-person data, i.e., the subject's verbal report about his inner experience during a simple visual task at the end of each single trial. That study also verified that the brain response is modulated by the background activity and showed that the fluctuations of subject's cognitive "context" defined by many parameters like attention and vigilance are a major source of variability. Interestingly, not only characteristic patterns of activation in different brain areas, but also characteristic patterns of synchrony between brain areas, were identified in the grouped responses indicating the role of long-range interactions in the response variability.

The present study has clearly demonstrated the nonstationary characteristics of the process underlying the response generation. The trial-to-trial nonstationarity has been recognized in previous studies involving neuromagnetic auditory (Liu and Ioannides, 1996; Laskaris and Ioannides, 2002) and somatosensory (Ioannides et al., 2002) responses. The new results reveal the contribution of the ongoing fluctuation to this nonstationarity. A functional role can be assigned to the background oscillatory activity (Brandt, 1997; Schurmann and Basar, 2001; Makeig et al., 2002; Penny et al., 2002), which is much more composite than usually described. Coherent oscillations have been found (Fries et al., 2001) to mediate the functional coupling of brain areas, which manifests itself in the form of stimulus-induced covariation. Recently the emergence of these oscillations has been assigned to feedback connections from higher brain regions and their role in shaping the responses of early sensory areas has started to be deciphered (Hupe et al., 2001; Galuske et al., 2002; Doiron et al., 2003; Gabbiani, 2003).

References

Arieli, A., Sterkin, A., Grinvald, A., Aertsen, A., 1996. Dynamics of ongoing activity: explanation of the large variability in evoked cortical responses. Science 273, 1868–1871.

Atukorale, A., Suganthan, P., 2000. Hierarchical overlapped neural gas network with application to pattern classification. Neurocomputing 35, 165–176.

Azouz, R., Gray, C.M., 1999. Cellular mechanisms contributing to response variability of cortical neurons in vivo. J. Neurosci. 19, 2209–2223.

Baumgartner, R., Somorjai, R., Summers, R., Richter, W., 2001. Ranking fMRI time courses by MSTs: assessing coactivation in fMRI. NeuroImage 13, 734–742.

Brandt, M., 1997. Visual and auditory evoked phase resetting of the alpha EEG. Int. J. Psychophysiol. 26, 285–298.

Brandt, M., Jansen, B., Carbonari, J., 1991. Pre-stimulus spectral EEG patterns and the visual evoked response. Electroencephalogr. Clin. Neurophysiol. 80, 16–20.

Choy, C., Siu, W., 1998. Fast sequential implementation of neural gas network for vector quantization. IEEE Trans. Commun. 46, 301–304.

Doiron, B., Chacron, M., Maler, L., Longtin, A., Bastian, J., 2003. Inhibitory feedback required for network oscillatory responses to communication but not prey stimuli. Nature 421, 539–543.

Duann, J., Jung, T., Kuo, W., Yeh, T., Makeig, S., Hsieh, J., Sejnowski, T., 2002. Single-trial variability in event-related BOLD signals. NeuroImage 15, 823–835.

Foxe, J., Simpson, G., 2002. Flow of activation from V1 to frontal cortex in humans. A framework for defining "early" visual processing. Exp. Brain Res. 142, 139–150.

Fries, P., Neuenschwander, S., Engel, A.K., Goebel, R., Singer, W., 2001. Rapid feature selective neuronal synchronization through correlated latency shifting. Nat. Neurosci. 4, 194–200.

Fukunaga, K., 1990. Introduction to Statistical Pattern Recognition, 2nd ED. Academic Press, Boston.

Gabbiani, F., 2003. A switch for oscillatory bursting. Nat. Neurosci. 6, 212–213.

Galuske, R., Schmidt, K., Goebel, R., Lomber, S., Payne, B., 2002. The role of feedback in shaping neural representations in cat visual cortex. Proc. Natl. Acad. Sci. USA 99, 17083–17088.

Good, P., 2000. Permutation Tests. Springer, New York.

Hjorth, B., 1975. An on-line transformation of EEG scalp potentials into orthogonal source derivations. Electroencephalogr. Clin. Neurophysiol. 39, 526–530.

Hupe, J., James, A., Girard, P., Lomber, S., Payne, B., Bullier, J., 2001. Feedback connections act on the early part of the responses in monkey visual cortex. J. Neurophysiol. 85, 134–145.

Ioannides, A.A., 1994. Estimation of brain activity using magnetic field tomography and large scale communication within the brain, in: Ho, M.W., Popp, F.A., Warnke, U. (Eds.), Bioelectronics and Biocommunication, World Scientific, Singapore, pp. 319–353.

Ioannides, A.A., Bolton, J., Clarke, C., 1990. Continuous probabilistic solutions to the biomagnetic inverse problem. Inverse Probl. 6, 523–542.

Ioannides, A.A., Taylor, J., Liu, L.C., Gross, J., Müller-Gärtner, H.W., 1998. The influence of stimulus properties, complexity, and contingency on the stability and variability of ongoing and evoked activity in human auditory cortex. NeuroImage 8, 149–162.

Ioannides, A.A., Kostopoulos, G., Laskaris, N., Liu, L.C., Shibata, T., Schellens, M., Poghosyan, V., Khurshudyan, A., 2002. Timing and connectivity in the human somatosensory cortex from single trial mass electrical activity. Hum. Brain Mapp. 15, 231–246.

Jain, A., Dubes, R., 1988. Algorithms for Clustering Data. Prentice Hall, Englewood Cliffs, NJ.

Jansen, B., Brandt, M., 1991. The effect of the phase of prestimulus alpha activity on the averaged visual evoked response. Electroencephalogr. Clin. Neurophysiol. 80, 241–250.

Jansen, B., Cheng, W., 1988. Structural EEG analysis: an explorative study. Int. J. Biomed. Comput. 23, 221–237.

Jung, T., Makeig, S., Westerfield, M., Townsend, J., Courchesne, E., Sejnowski, T., 2001. Analysis and Visualization of single-trial event-related potentials. Hum. Brain Map. 14, 166–185.

Kangas, J.A., Kohonen, T., Laaksonen, J., 1990. Variants of self-organizing maps. IEEE Trans. Neural Networks 1, 93–99.

Kisley, M., Gerstein, G., 1999. Trial-to-trial variability and state-dependent modulation of auditory-evoked responses in cortex. J. Neurosci. 19, 10451–10460.

Ktonas, P., Paparrigopoulos, M., Manoyiou, B., Bergiannaki, M., Soldatos, C., 2000. Sleep spindle incidence dynamics: a pilot study based on a markovian analysis. Sleep 23, 419–423.

Laskaris, N.A., Ioannides, A.A., 2001. Exploratory data analysis of evoked response single trials based on minimal spanning tree. Clin. Neurophysiol. 112, 698–712.

Laskaris, N.A., Ioannides, A.A., 2002. Semantic geodesic maps: a unifying geometrical approach for studying the structure and dynamics of single trial evoked responses. Clin. Neurophysiol. 113, 1209–1226.

Liu, L.C., Ioannides, A.A., 1996. A correlation study of averaged and single trials MEG signals: the average describes multiple histories each in a different set of single trials. Brain Topogr. 8, 385–396.

Liu, L.C., Ioannides, A.A., Müller-Gärtner, H.W., 1998. Bi-hemispheric study of single trial MEG signals of the human auditory cortex. Electroenceph. Clin. Neurophysiol. 106, 64–78.

Lutz, A., Lachaux, J., Martinerie, J., Varela, F., 2002. Guiding the study of brain dynamics by using first-person data: synchrony patterns correlate with ongoing conscious states during a simple isual task. Proc. Natl. Acad. Sci. USA 99, 1586–1591.

Makeig, S., Westerfield, M., Jung, T.-P., Enghoff, S., Townsend, J., Courchesne, E., Sejnowski, T., 2002. Dynamic brain sources of visual evoked responses. Science 295, 690–694.

Martinez, T., Schulten, K., 1994. Topology representing networks. Neural Networks 7, 507–522.

Mast, J., Victor, J., 1991. Fluctuations of steady-state VEPs: interaction of driven evoked potentials and the EEG. Electroenceph. Clin. Neurophysiol. 78, 389–401.

Moradi, F., Liu, L.C., Cheng, K., Waggoner, R.A., Tanaka, K., Ioannides, A.A., 2003. Consistent and precise localization of brain activity in human primary visual cortex by MEG and fMRI. NeuroImage 18, 595–609.

Penny, W., Kiebel, S., Kilner, J., Rugg, M., 2002. Event-related brain dynamics. Trends Neurosci. 25, 387–389.

Raiguel, S.E., Lagae, L., Gulyas, B., Orban, G.A., 1989. Response latencies of visual cells in macaque areas V1, V2 and V5. Brain Res 493, 155–159.

Reich, D.S., Victor, J.D., Knight, B.W., Ozaki, T., Kaplan, E., 1997. Response variability and timing precision of neuronal spike trains in vivo. J. Neurophysiol. 77, 2836–2841.

Russo, F., Martinez, A., Sereno, M., Pitzalis, S., Hillyard, S., 2001. Cortical sources of the early components of the visual evoked potential Hum. Brain Mapp. 15, 95–111.

Schurmann, M., Basar, E., 2001. Functional aspects of alpha oscillations in the EEG. Int. J. Psychophysiol. 39, 151–158.

Tallon-Baudry, C., Bertrand, O., Delpuech, C., Pernier, J., 1996. Stimulus specificity of phase-locked and non-phase-locked 40 Hz visual responses in human. J. Neurosci. 16, 4240–4249.

Thorpe, S., Fize, D., Marlot, C., 1996. Speed of processing in the human visual system. Nature 381, 520–522.

Truccolo, W., Ding, M., Knuth, K., Nakamura, R., Bressler, S., 2002. Trial-to-trial variability of cortical evoked responses: implications for the analysis of functional connectivity. Clin. Neurophysiol. 113, 206–226.

Tzelepi, A., Ioannides, A.A., Poghosyan, V., 2001. Early (N70m) neuromagnetic signal topography and striate and extrastriate generators following pattern onset quadrant stimulation. NeuroImage 13, 702–718.

Vanni, S., Tanskanen, T., Seppa, M., Uutela, K., Hari, R., 2001. Coinciding early activation of the human primary visual cortex and anteromedial cuneus. Proc. Natl. Acad. Sci. USA 98, 2776–2780.

Yager, R., Filev, D., 1994. Generation of fuzzy rules by mountain clustering. J. Intell. Fuzzy Syst. 2, 209–219.